A High-Accuracy, Low-Order Thermal Model of SiC MOSFET Power Modules Extracted from Finite Element Analysis via Model Order Reduction

Cameron Entzminger, Wei Qiao, Liyan Qu, and Jerry L. Hudgins
Department of Electrical and Computer Engineering
University of Nebraska-Lincoln
Lincoln, NE 68588-0511 USA
centzminger@unomaha.edu; wqiao3@unl.edu; lqu2@unl.edu; hudgins@engr.unl.edu

Abstract— **Silicon carbide (SiC) MOSFET power modules are being used for high power applications because of their superior thermal characteristics and high blocking voltage capabilities over traditional silicon power modules. This paper explores modeling the thermal process of a SiC MOSFET power module through a high-order finite element analysis (FEA) based thermal model and then reducing the order of the FEA thermal model using a Krylov subspace method. The low-order thermal model has a significantly reduced computation cost compared to the FEA model while preserving the accuracy of the model. The proposed method is applied to generate low-order thermal models for a SiC MOSFET, which are validated by computer simulations with respect to the FEA thermal model.**

Keywords—Krylov subspace projection, metal–oxide–semiconductor field-effect transistor (MOSFET), model order reduction, power module, silicon carbide (SiC), thermal modeling

I. Introduction

Power modules contain power semiconductors which are used for high power applications, such as three-phase inverters in medium-voltage drives or wind turbines. Recently, silicon carbide (SiC) metal–oxide–semiconductor field-effect transistor (MOSFET) power modules have been used for their efficient thermal conductivity characteristics and high blocking voltage capabilities [1]. Factors such as electrical stresses, power cycling, and mechanical vibration all contribute to the deterioration of the power semiconductors inside power modules [2], [3]. The power semiconductors are mounted on different layers of materials inside modules, which provide efficient thermal dissipation for the semiconductor chips and electrical isolation from the mounting baseplate [4], [5]. The mismatch of thermal expansion coefficients between the different materials used in the semiconductor mounting layers causes each layer to expand by a different amount during a power cycling event, which creates mechanical stresses at the interfaces between mismatched layers. Existing cracks in the solder layers grow with each thermal expansion event due to these mechanical stresses [6]. Growing cracks can manifest as changes in the heat conduction path from the semiconductor chip to the baseplate or in bond wire lift-off [7]. These changes can result in failure of the device. Changes in the heat conduction path of the semiconductor chip to the baseplate heat sink can act as a failure indicator for power module. Therefore, a high accuracy thermal model of a SiC MOSFET power module is needed to monitor for these failure indicators.

An ideal thermal model has high accuracy and low computational complexity. Thermal equivalent circuits [8]-[11] are widely used for modeling power modules. This method models each layer of a power module as a resistor and capacitor pair of thermal resistance and lumped thermal capacitance. With only seven layers in a standard power module topology, this results in seven resistor and capacitor pairs, or a seventh order system of equations. The method oversimplifies the capacitances of some thick layers of modules such as the baseplate [12]. This results in a less accurate temperature estimation during transient heating events. Finite element methods can solve for the temperature distribution across a discretized power module model with a high degree of accuracy for both steady-state and transient events. However, this method is computationally complex because for a complicated and finely meshed model, there are typically more than thousands of degrees of freedom (DoFs) to solve for. The order of the model is equal to the total number of DoFs at each node. A state-space representation of a finite element model can be extracted from simulation software. Model order reduction (MOR) techniques can be applied to this state-space model to reduce the order of the system while preserving the dominant eigenvalues of the system matrices thus preserving the behavior of the system with a controllable approximation error [13]. Therefore, an accurate low-order state-space model from an extracted finite element model can be used to monitor the temperature distribution across a SiC MOSFET power module.

There are different ways to approximate large-scale dynamic systems using MOR. Hankel singular values measure the contribution of each state variable in a system to the input-output behavior. By discarding low contributing states of a system, the input-output behavior can be preserved while reducing the computational complexity of the model. The system can then be reduced to an order which meets a desired approximation error bound. However, the computational complexity of this method of MOR grows cubically as the initial system order increases [13]. Therefore, this method is applicable for low-order systems only. For high-order systems

This work was supported in part by the U.S. National Science Foundation under Grant CMMI-1663562.

consisting of large sparse matrices, Krylov subspace methods can be used for MOR.

This paper proposes a Krylov subspace based MOR method for generating low-order state-space thermal models for SiC MOSFET power modules. In the proposed method, the Arnoldi iteration algorithm is applied to compute an orthogonal projection matrix of lower order, which can be used to project the high-order system matrices onto the lower-order Krylov subspace. The orthogonal projection matrix is then applied to a high-order finite element thermal model of a SiC MOSFET power module to extract an accurate low-order state-space thermal model for the power module. The proposed MOR method uses a mathematical approximation process without any heuristic assumptions. The extracted low-order state-space thermal model is computational efficient and has a controllable error bound with respect to the high-order system. The proposed MOR method is validated by thermal modeling results for a SiC MOSFET power module.

II. Proposed Thermal Model

Finite element analysis (FEA) is commonly used to model physical phenomenon with a high degree of accuracy. A finite element simulation is set up by first importing a geometric model. Then, a set of governing equations is chosen for the model depending on the physics involved. For a heat transfer problem, the following governing equation can be formulated to model the thermal process.

$$-\left(\frac{\partial q_x}{\partial x}+\frac{\partial q_y}{\partial y}+\frac{\partial q_z}{\partial z}\right)+Q=\rho c\frac{\partial T}{\partial t} \tag{1}$$

where q_x, q_y, and q_z are the heat fluxes in each direction, Q is the heat generation, ρ is the density, and c is the specific heat capacity.

Next, boundary conditions and initial conditions are applied to the model. Using the Galerkin method, the model can be discretized into a set of elements called a mesh. Using finite element software to implement the Galerkin method, the parameters of the fidelity of the meshed model can be controlled. The resulting relationship between the material properties, the number of discretized nodes, the boundary conditions, and initial constraints can be shown in Equation (2).

$$[C]\{\dot{T}\}+[K]\{T\}=\{F\} \tag{2}$$

where the $n \times n$ matrices $[C]$ and $[K]$ are the specific heat capacity and thermal conductivity relationships between each of the nodes in the finite element model, respectively; n is the number of DoFs in the model; the vector $\{T\}$ represents all the nodal temperatures; and the vector $\{F\}$ is the summation of each heat generation, conductive heat flux, and convective heat flux boundary conditions applied to the model. For each node, there is only one DoF, which is temperature.

Data comprised in Equation (2) can be rewritten into a state-space representation of a linear system relating the inputs, outputs, and state variables as follows.

$$\begin{cases}\dfrac{dx}{dt}=([M]^{-1}[A])x+([M]^{-1}[B])u\\ y=[C]x+[D]u\end{cases} \tag{3}$$

Table I: State-Space System Dimensions for Full-Order and Reduced-Order Models.

Matrix or Vector	Full-Order System Dimensions	Reduced-Order System Dimensions
$[A]$	$n \times n$	$m \times m$
$[B]$	$n \times Inputs$	$m \times Inputs$
$[C]$	$Outputs \times n$	$Outputs \times m$
$[D]$	$Outputs \times Inputs$	$Outputs \times Inputs$
x	$n \times 1$	$m \times 1$
y	$Outputs \times 1$	$Outputs \times 1$
u	$Inputs \times 1$	$Inputs \times 1$
$[M]$	$n \times n$	$m \times m$

where the vector x represents the state variables or the nodal temperatures of the model; the vector u represents the time varying model inputs such as heat flux or heat generation; the vector y represents the time varying output temperatures as a result of the input and state characteristics; the mass matrix $[M]$ contains information for nodal thermal heat capacity; the system matrices $[A]$, $[B]$, $[C]$, and $[D]$ control the effects of the state variables to other state variables, the input's effect on the state variables, the state variables influence on the selected outputs, and the input's effect on the selected outputs, respectively. The dimensions of each vector and system matrix are shown in Table I, where n is the number of DoFs in the extracted system, or the system's order.

Using the Arnoldi iteration, the extracted full-order state-space model can be reduced to a chosen system order. The Arnoldi iteration finds an approximation of the dominant eigenvalues of a matrix by constructing an orthonormal basis of the Krylov subspace of the matrix. Starting with the initial system matrix of a state-space system and an initial starting vector, a Krylov subspace of a specified order can be generated. The Arnoldi iteration produces a sequence of orthonormal vectors that span the Krylov subspace. Each generated vector of the Krylov subspace is normalized using the Gram-Schmidt orthogonalization process, which results in an orthogonal basis of the Krylov subspace. This resulting matrix $[V]$, of $n \times m$ dimension, where m ($m << n$) is the desired reduction order, is a projection matrix that can be used to project each matrix in a state-space system onto a low-order dimensional space. The resulting reduced-order system dimensions can be seen in Table 1. The original state vector x is equal to the projection matrix $[V]$ multiplied by a lower order vector z. The resulting state-space system as seen in Equation (4) is a reduced-order system based on the extracted full-order finite element model.

$$\begin{cases}\dfrac{dz}{dt}=[V]^T([M]^{-1}[A])[V]z+[V]^T([M]^{-1}[B])u\\ y=[C][V]z+[D]u\end{cases} \tag{4}$$

III. Results and Discussion

Computer simulations were carried out for thermal modeling of a six-pack SiC MOSFET power module to validate the proposed thermal model. The six-pack power module consists of six switches and six free-wheeling diodes used for three-phase applications. Each semiconductor chip and diode are mounted on the baseplate through a series of

Table II: Power Module Layer Geometries and Material Properties.

Power Module Material Layer	Length (mm)	Width (mm)	Thickness (mm)	Thermal Conductivity (W/mK)	Density (kg/^3)	Specific Heat Capacity (J/(kg*K))	Thermal Resistance (W/mK)	Thermal Capacitance (J/K)
Chip (MOSFET)	5	5	0.18	5	5	0.18	0.06	0.001
Solder (MOSFET)	5	5	0.05	5	5	0.05	0.04	0.0018
Chip (Diode)	4.14	6.38	0.38	4.14	6.38	0.38	0.1199	0.0023
Solder (Diode)	4.14	6.38	0.05	4.14	6.38	0.05	0.0379	0.0019
Copper (Top)	9.154	14.54	0.28	9.154	14.54	0.28	0.0052	0.1282
Aluminum Nitride	23.6	31.24	0.68	23.6	31.24	0.68	0.0051	0.1209
Copper (Bottom)	23.6	31.24	0.05	23.6	31.24	0.05	0.0009	0.71
Solder (Baseplate)	23.6	31.24	0.05	23.6	31.24	0.05	0.0014	0.0517
Copper (Baseplate)	107.5	45	3	107.5	45	3	0.0093	49.91

different material layers. First, the conducting aluminum bond wires are mounted to the tops of the SiC semiconductor chips. The chips are soldered to an aluminum nitride (AlN) ceramic layer surrounded by copper plating. This ceramic layer provides electrical isolation of the chip from the baseplate while also conducting a large amount of heat from the chip while having a small thermal expansion coefficient. The bottom copper layer was then soldered to the large copper baseplate. The collected geometries and linear material properties of the SiC MOSFET power module are compiled in Table II. The packaging, terminal busbars, and silicone gel were not considered for this model. The silicone gel has a much lower thermal conductivity (0.2 W/mΩ*K) than the surrounding metals which acts as thermal insulation for the semiconductor chips [14]. During module operation, the heat generated at the semiconductor chips is conducted through the material layers to the baseplate.

The power loss curves of the SiC MOSFETs and SiC diodes were developed from the device characteristics and operational parameters of a switch used in a three-phase inverter circuit with an induction motor load, which was designed in MATLAB/Simulink with the add-on Simscape. Device properties such as turn-on and turn-off energies and on-state resistance were obtained from the CREE CCS050M12CM2 datasheet, which is an all SiC six-pack power module. A sine-triangle pulse-width modulation switching scheme was used with the inverter to drive the induction motor load. The inverter used a 400 V DC-link voltage, 60 A peak sinusoidal output current, 5 kHz switching frequency, and 60 Hz line frequency. Simscape MOSFET and diode models were used for the simulation because the power loss during operation can be directly extracted from these models. The resulting power loss for the MOSFETs and diodes are shown in Fig. 1.

COMSOL Multiphysics was used for FEA. A power module in operation has several heat constraints, such as the cooling convection force of the mounted heat sink, the heat generation from the semiconductor chips and diodes, the thermal insulation of the packaging silicone gel, and the ambient temperature of the operating environment. The cooling convection coefficient was chosen to be a value of 10,000 W/m^2K, which is a standard value for a liquid cooling heat sink system [15]. The ambient operational temperature of the device was chosen to be 60 °C. The thermal insulation of the packaging silicone gel was used as a thermal insulation barrier due to the much lower thermal conductivity of the material compared to the copper baseplate packaging. The software COMSOL LiveLink for MATLAB is an interfacing software used to run the COMSOL API within MATLAB. The command mphstate was used to extract a full-order state space model from COMSOL into a MATLAB object. There were twelve input power loss curves, six MOSFETs, two for each inverter leg, and six free-wheeling diodes for each MOSFET. Each power loss curve was applied as a heat flux constraint to the top of the corresponding MOSFET or diode in the model. Four temperature plots were output using simulation probes at the center of the top and bottom MOSFETs and diodes used for the first inverter leg.

Shown in Fig. 2 is the three-dimensional (3-D) temperature plot of the SiC MOSFET power module with time varying heat flux loads obtained from a 3-D full-order finite element thermal model in COMSOL. Fig. 3 shows the alternating temperature profiles of top and bottom MOSFETs obtained from the full-order thermal model compared with the low-order simulation. The top MOSFET temperature fluctuates in the range of 20-25 °C. The magnitude of the temperature change decreases over time as the inverter settles to a sinusoidal steady-state output. The bottom MOSFET fluctuates in the range of 15-20 °C and this fluctuation magnitude increases

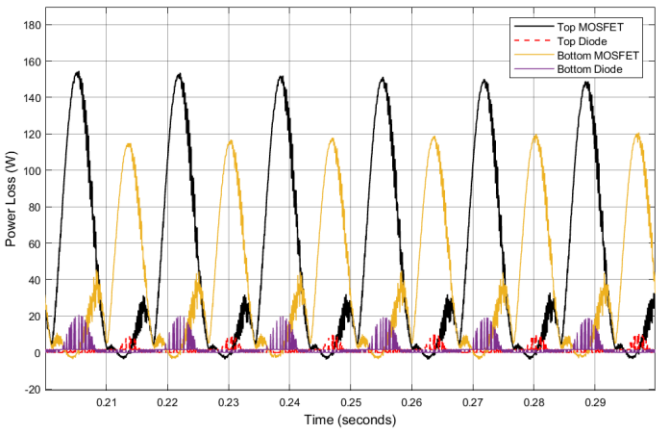

Fig. 1. Power loss curves for MOSFETs and diodes.

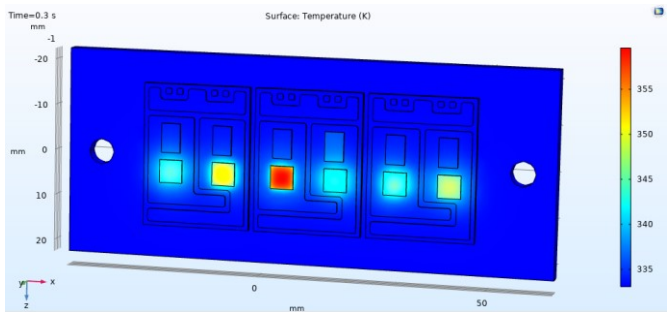

Fig. 2. 3-D temperature plot of the SiC MOSFET power module in COMSOL.

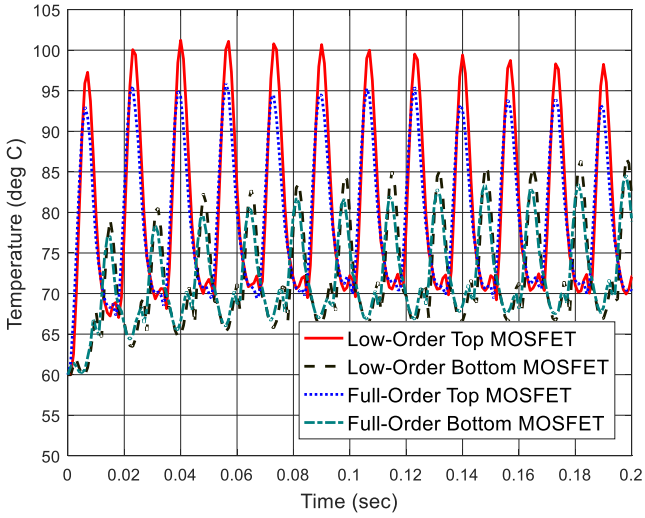

Fig. 3. MOSFET chip temperature plots obtained from full-order and reduced 20-order model.

towards a steady state as well. The peak temperature above the initial temperature was about 98 °C, which was 38 °C above the ambient temperature. The temperature profile is based on the total thermal conductivity, specific heat capacity, linearity of the materials used, and the thermal boundary conditions. The power loss curves for the MOSFETs and diodes are dependent on the switching frequency, the turn-on and turn-off energies, the on-state resistance of the semiconductor devices, and the operating currents and voltages of the devices. In COMSOL, the solved solution is dependent on solver settings and mesh quality. Nonlinear material properties that are dependent on temperature would improve the accuracy of the temperature distribution simulation. The full-order state-space model with a system order of 31,026 was reduced to a system order of 20 using the proposed method. The low-order model was solved for two multiple-input single-output scenarios for both the top middle and bottom middle MOSFETs to obtain their temperature curves, as shown in Fig. 3.

The error introduced to the model originates from the mathematical approximation error within the Arnoldi iteration used to reduce the order of the state-space system. The higher the order number, the less approximation error introduced into the state-space system. However, increasing the order number increases the necessary computation time to solve the model. The approximation error between the full-order system and the

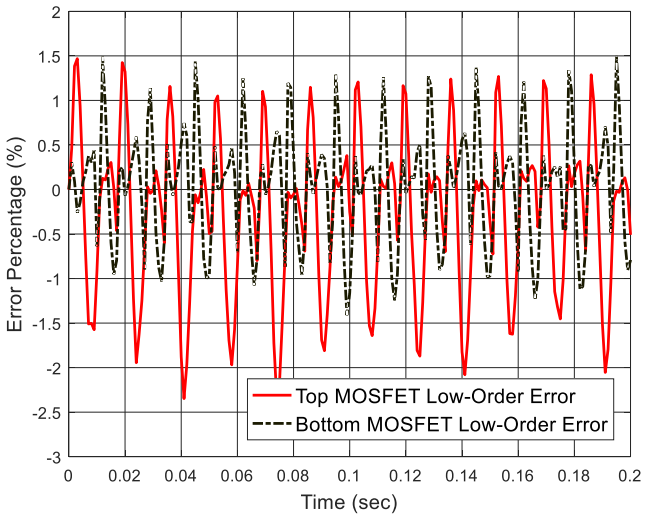

Fig. 4. Approximation error of the reduced 20-order model for top and bottom MOSFET chip temperatures.

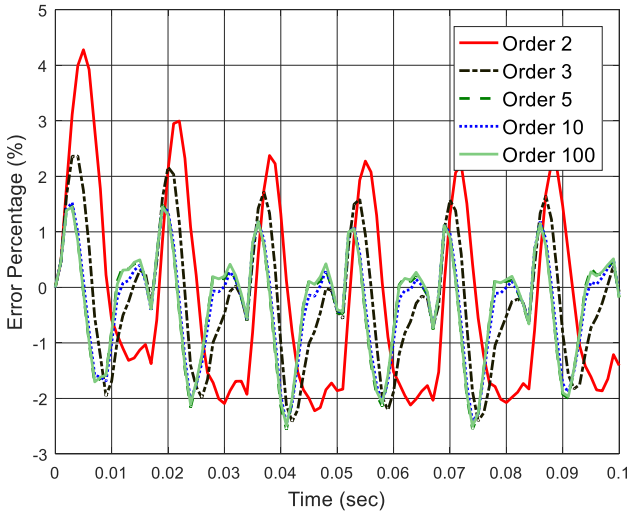

Fig. 5. Approximation error of multiple reduction orders.

reduced low-order system is less than 2.4% and 1.5% for the top and bottom MOSFET, respectively, as shown in Fig. 4. The base value for the approximation error calculation was the COMSOL solver solution. The reduced-order model took seconds to solve compared to the days it took to solve the full-order state-space system extracted from COMSOL in MATLAB.

The approximation error over time for multiple reduction orders can be seen in Fig. 5, where the lowest reduction order yields the highest maximum error. The average, maximum, and minimum error as the reduction order increases can be seen in Fig. 6. Increasing the fidelity of the mesh in COMSOL increases the full-order system order. Three different starting full-order system orders were compared in Fig. 6: 31026, 42713, and 91774. The maximum error stays below 2.5% for all full-order systems above a reduction order of 15 and rises sharply as order tends towards zero. The average error stays below 1% for all tested full-order systems above a reduction order of 5.

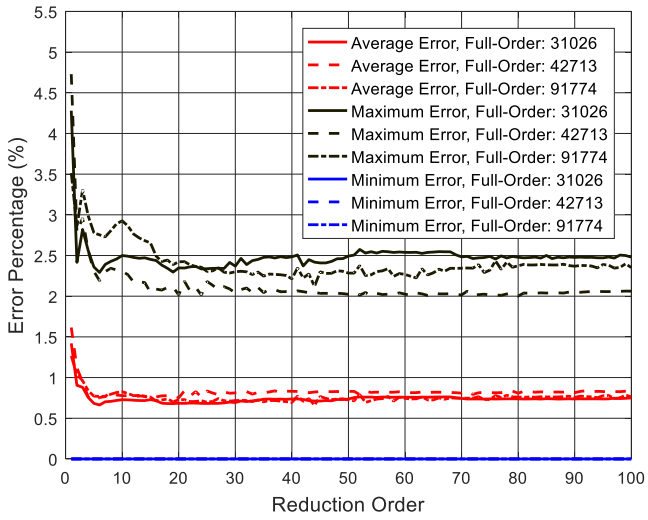

Fig. 6. Reduction order vs. average, maximum, and minimum error.

IV. Conclusions

This study explored the effectiveness of modeling the thermal process of a SiC MOSFET power module with a low-order state-space model created by using a Krylov subspace projection method for reducing a high-order state-space model generated from the FEA method without any heuristic assumptions. The low-order thermal model extracted by using the proposed method has a controllable approximation error with respect to the most accurate FEA thermal model, which depends on the order number chosen for the MOR. The modeling parameters and considerations for creating a SiC MOSFET power module were considered as well as creating the necessary heat generation and cooling constraints for the model. The trade-offs of choosing a low system order were discussed and verified through simulation. The future work for this study lies in developing a mathematical relationship between the desired approximation error introduced due to the Arnoldi iteration method and the resulting system order. Based on the mathematical relationship, a method to determining the tradeoff between model order and error will be investigated. More simulation studies and experimental tests on a specific SiC MOSFET power module will be carried out to further verify the low-order thermal model generated by the proposed method under various operating conditions.

V. References

[1] J. Millan, P. Godignon, X. Perpina, A. Perez-Tomas, and J. Rebollo, "A survey of wide bandgap power semiconductor devices," *IEEE Trans. Power Electronics*, vol. 29, no. 5, pp. 2155–2163, May 2014.

[2] M. Ciappa, "Selected failure mechanisms of modern power modules," *Microelectronics Reliability*, vol. 42, no. 4–5, pp. 653–667, 2002.

[3] B. Lu and S. K. Sharma, "A literature review of IGBT fault diagnostic and protection methods for power inverters," *IEEE Trans. Industry Applications*, vol. 45, no. 5, pp. 1770–1777, Sept.-Oct. 2009.

[4] Z. J. Shen and I. Omura, "Power semiconductor devices for hybrid, electric, and fuel cell vehicles," *Proc. IEEE*, vol. 95, no. 4, pp. 778–789, 2007.

[5] T. K. Gachovska, B. Tian, J. L. Hudgins, W. Qiao, and J. F. Donlon, "A real-time thermal model for monitoring of power semiconductor devices," *IEEE Trans. Industry Applications,* vol. 51, no. 5, pp. 3361-3367, July. 2015.

[6] A. Morozumi, K. Yamada, T. Miyasaka, S. Sumi, and Y. Seki, "Reliability of power cycling for IGBT power semiconductor modules," *IEEE Trans. Industry Applications*, vol. 39, no. 3, pp. 665–671, May-Jun. 2003.

[7] Z. Wang, W. Qiao, B. Tian, and L. Qu, "An effective heat propagation path-based online adaptive thermal model for IGBT modules," in *Proc. IEEE Applied Power Electronics Conf. Expo*., 2014, pp. 513–518.

[8] A. Castellazzi, "Comprehensive compact models for the circuit simulation of multichip power modules," *IEEE Trans. Power Electron.*, vol. 25, no. 5, pp. 1251–1264, May 2010.

[9] M. Musallam and C. M. Johnson, "Real-time compact thermal models for health management of power electronics," *IEEE Trans. Power Electron.*, vol. 25, no. 6, pp. 1416–1425, Jun. 2010.

[10] P. L. Evans, A. Castellazzi, and C. M. Johnson, "Automated fast extraction of compact thermal models for power electronic modules," *IEEE Trans. Power Electron.*, vol. 28, no. 10, pp. 4791–4802, Oct. 2013.

[11] K. Ma, A. S. Bahman, S. Beczkowski, and F. Blaabjerg, "Complete loss and thermal model of power semiconductors including device rating information," *IEEE Trans. Power Electron.*, vol. 30, no. 5, pp. 2556-2569, May 2015.

[12] Z. Wang and W. Qiao, "A physics-based improved Cauer-type thermal equivalent circuit for IGBT modules," *IEEE Trans. Power Electronics*, vol. 31, no. 10, pp. 6781–6786, Oct. 2016.

[13] E. B. Rudnyi and J. G. Korvink, "Review: Automatic model reduction for transient simulation of MEMS-based devices," *Sensors Update*, vol. 11, no. 1, pp. 3–33, 2002.

[14] Q. Mu, S. Feng, and G Diao, "Thermal conductivity of silicone rubber filled with ZnO," *Polym. Compos,* vol. 28, no. 2, pp. 125-130, Feb. 2007.

[15] T. L. Bergman, A. S. Lavine, F. P. Incropera, and D. P. Dewitt, *Fundamentals of Heat and Mass Transfer,* John Wiley & Sons, Inc., Danvers, MA, 2011.